Density functional theory study of phase IV of solid hydrogen

Chris J. Pickard* and Miguel Martinez-Canales
Department of Physics & Astronomy, University College London, Gower Street, London WC1E 6BT, UK

Richard J. Needs
Theory of Condensed Matter Group, Cavendish Laboratory, Cambridge CB3 0HE, UK
(Received 15 April 2012; revised manuscript received 14 May 2012; published 15 June 2012)

We have studied solid hydrogen up to pressures of 300 GPa and temperatures of 350 K using density functional theory methods and have found "mixed structures" that are more stable than those predicted earlier. Mixed structures consist of alternate layers of strongly bonded molecules and weakly bonded graphene-like sheets. Quasiharmonic vibrational calculations show that mixed structures are the most stable at room temperature over the pressure range 250–295 GPa. These structures are stabilized with respect to strongly bonded molecular phases at room temperature by the presence of lower frequency vibrational modes arising from the graphene-like sheets. Our results for the mixed structures are consistent with the experimental Raman data [M. I. Eremets and I. A. Troyan, Nat. Mater. **10**, 927 (2011) and R. T. Howie *et al.*, Phys. Rev. Lett. **108**, 125501 (2012)]. We find that mixed phases are reasonable structural models for phase IV of hydrogen.

DOI: 10.1103/PhysRevB.85.214114 PACS number(s): 62.50.−p, 64.70.K−, 61.50.Ks, 71.15.Mb

I. INTRODUCTION

Hydrogen is the most abundant and ancient element in the universe and the simplest of all atoms. Hydrogen was solidified by Dewar,[1] and Wigner and Huntington predicted that solid hydrogen would metallize at pressures of about 25 GPa,[2] although the metallization pressure is now known to be much higher. Insulating molecular phases of solid hydrogen have been identified in static diamond anvil cell (DAC) experiments up to pressures of over 300 GPa. Phase I is a quantum crystal consisting of rotating hydrogen molecules on a hexagonal close packed lattice.[3] The orientationally ordered molecular phases II and III[4] appear at pressures of about 110 and 150 GPa, respectively,[3] but their structures have not been determined experimentally. Ashcroft suggested that metallic hydrogen might superconduct up to room temperature[5] and, more recently, possible superconducting superfluids and metallic superfluids of hydrogen have been suggested.[6] The gas giants Jupiter and Saturn and some of the recently discovered extrasolar planets[7] are believed to contain large amounts of metallic hydrogen at high temperatures and pressures into the terapascal range. Metallic hydrogen has been generated at temperatures of several thousand kelvins in dynamic shock wave experiments,[8] but it has proved very difficult to form metallic hydrogen at lower temperatures in DACs.

DAC studies at pressures up to 300 GPa are approaching current experimental limits. Determining crystalline structures of hydrogen at high pressures is extremely difficult because x-ray diffraction, which is the workhorse of crystal structure determination, is severely hampered by the weak scattering of hydrogen.[9,10] Raman[3,11,12] and infrared (IR)[3,13] vibrational spectroscopies have been very important in studying the bonding and structures of hydrogen at high pressures, although they have not proved sufficient to determine the structures themselves.

Recent room temperature (295–300 K) DAC experiments up to pressures of around 300 GPa have found evidence for a previously unreported structural phase of hydrogen, which we refer to as the putative phase IV.[14,15] The intense Raman molecular vibron mode started to drop rapidly in frequency as the pressure was increased above about 200 GPa, and at higher pressures the samples became dark.[14,15] Darkening of samples above 200 GPa was observed in earlier low-temperature experiments,[12,16] suggesting a reduction in the band gap that may be a precursor to metallization. Darkening was also observed at high pressures in Refs. 14 and 15. Eremets and Troyan reported an increase in electrical conductance around 260–270 GPa.[14] The Raman data in Refs. 14 and 15 are similar, although in Ref. 15 signals characteristic of phase IV were obtained up to higher pressures of 315 GPa. The Raman data of Refs. 14 and 15 can be used to eliminate candidate structures for phase IV. There are differences between these experimental data, but here we focus on quantities for which there is a reasonable degree of consistency between the studies.

In previous work[17,18] we searched for high-pressure structures of hydrogen using density functional theory (DFT) methods and *ab initio* random structure searching (AIRSS).[19,20] Structures were found at pressures from about 80 to nearly 400 GPa which were calculated to be more stable than previously known ones. Several candidates for phase II were found, although the enthalpy differences between them are very small. A single outstanding candidate of $C2/c$ symmetry was found for phase III.[17] This structure was the lowest in enthalpy from about 70–250 GPa when proton zero-point (ZP) motion was included, which covers most of the region in which phase III is observed. The $C2/c$ structure also exhibits strong IR activity that is characteristic of phase III,[13,21] and it gives a good account of the Raman-active vibron frequency. A molecular structure of $Cmca$ symmetry was found to be stable in the range 250–380 GPa, which we refer to as $Cmca$-12, where the "12" denotes the number of atoms in the primitive unit cell. Above 380 GPa another structure of $Cmca$ symmetry[22] was the most stable, which we refer to as $Cmca$-4. The discovery of a class of "mixed" hydrogen structures consisting of alternate layers of strongly bonded molecules and weakly bonded graphene-like sheets was reported in Ref. 17. Mixed structures with $Pbcn$, $C2$, and $Ibam$ symmetries were found

and, when ZP motion was included, $Pbcn$ in particular became energetically competitive with the $C2/c$ phase over a wide range of pressures.[17]

In this work we have used AIRSS to identify candidate structures for phase IV. In the AIRSS approach randomly chosen structures are relaxed to minima in the enthalpy.[19,20] The basic AIRSS method has virtually no free parameters and is essentially unbiased, and it is therefore an ideal starting point from which to introduce useful biases and constraints. The most important technical improvements on the searches of Refs. 17 and 18 are that here we employ constraints to exclude very low symmetry structures which, according to Pauling's rule of parsimony,[23] are unlikely to be low in enthalpy, and that we have "shaken" low-enthalpy structures by making small random atomic displacements and re-relaxing. We have also shaken supercells of low-enthalpy structures that are then able to relax into structures with the larger supercell periodicity. AIRSS has been applied to many systems including molecular solids such as hydrogen,[17,24] water,[25] nitrogen,[26] ammonia,[27] and ammonia monohydrate.[28]

II. DESCRIPTION OF THE CALCULATIONS

A. DFT calculations

Our main DFT calculations were performed with the CASTEP[29] code, the Perdew-Burke-Ernzerhof (PBE)[30] generalized gradient approximation (GGA) density functional, and ultrasoft pseudopotentials.[31] For the searches we used a standard ultrasoft pseudopotential, a plane wave cutoff energy of 230 eV, and a Monkhorst-Pack[32] Brillouin zone sampling grid of spacing $2\pi \times 0.05$ Å^{-1}. The structures obtained in the searches were re-relaxed at a higher level of accuracy consisting of a hard ultrasoft pseudopotential, a plane wave cutoff energy of 1000 eV, and a Brillouin zone sampling grid of spacing $2\pi \times 0.03$ Å^{-1}. The enthalpies of the structures reported in the paper were calculated at the higher level of accuracy. For the phonon, Raman, and IR calculations we used a plane wave cutoff energy of 1200 eV and Brillouin zone sampling grids of spacing $2\pi \times 0.04$ Å^{-1}. The phonon calculations were performed with the CASTEP code and cross-checked with the Quantum ESPRESSO code.[33]

B. AIRSS calculations

We have performed AIRSS runs in addition to those reported in our earlier papers.[17,18] The searches were performed at 250 GPa unless otherwise specified. Searches in 24 and 48 atom cells using symmetry constraints with from 2 up to 12 symmetry operations were performed, and 4956 relaxed structures were obtained. These structures included the important Pc structure (Fig. 1) which was found in searches with 2 symmetry operations. The 16-atom $Ibam$ mixed structure[17] was shaken in supercells with up to 96 atoms, and 305 relaxed structures were obtained. The 48-atom $Pbcn$ mixed structure was shaken in supercells with up to 192 atoms, giving 156 relaxed structures, and the Pc structure was also found in these searches. The 24-atom $C2/c$ structure was shaken in supercells with up to 96 atoms and 253 relaxed structures were obtained, and the 48-atom Pc structure was shaken in supercells with up to 192 atoms at 300 and 350 GPa, giving 333 relaxed structures. We also found the $Cmca$-12 and $Cmca$-4 structures in our searches. Note that the $C2/c$ structure that is our best candidate for phase III has 24 atoms in the primitive unit cell[17] and that it is different from the $C2/c$ structure found by Tse *et al.*,[34] which has 12 atoms in the primitive unit cell. In the supplementary information for Ref. 17 our 24-atom $C2/c$ structure was referred to by an alternative setting of $B2/n$. The two $C2/c$ structures differ in the stacking of layers, and the 24-atom structure is lower in enthalpy.

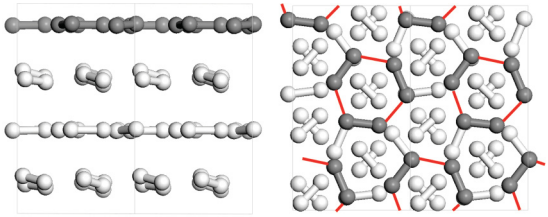

FIG. 1. (Color online) Side and top views of the Pc structure at 250 GPa. The side view shows the four-layer repeat with a weakly bonded graphene-like layer on top (shaded atoms). The red lines show the next-nearest contacts within the layer.

III. RESULTS

A. Structure searches

The searches confirmed our previous results,[17] but we also found the Pc symmetry mixed phase which has 48 atoms in the primitive unit cell.[35] The Pc structure is similar to $Pbcn$, but with a somewhat larger distortion of the graphene-like layers; see Fig. 1. Static lattice DFT calculations show Pc to be about 2 meV per atom more stable than $Pbcn$, and at 200 GPa it is only about 3 meV per atom higher in enthalpy than $C2/c$. We emphasize that the enthalpy differences between competing

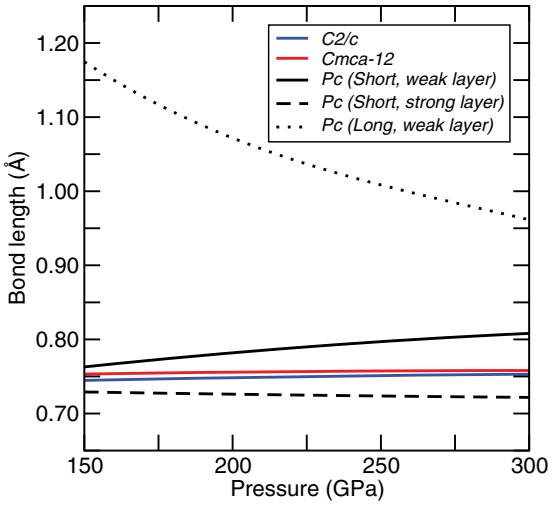

FIG. 2. (Color online) Evolution of the bond lengths of $C2/c$, $Cmca$-12, and Pc with pressure. The molecular bond lengths of $C2/c$ and $Cmca$-12 slowly expand with increasing pressure, while the short bonds in the strong layers of Pc undergo a slight contraction. The most notable feature is the behavior of the bonds in the weak layers. The short bonds in the weak layers expand with pressure rather more rapidly than those of $C2/c$ and $Cmca$-12, while the long bonds in the weak layers contract rapidly with pressure.

phases are particularly small in hydrogen, with shifts of order 1 meV per atom leading to significant changes in the numerical results. Howie *et al.*[15] recognized that the Raman data for phase IV might be explained by a mixed structure such as *Pbcn*, based on the calculated data reported in Ref. 17.

B. Bond lengths of the structures

As shown in Fig. 2, the shortest bonds in $C2/c$ and *Cmca*-12 at 150 GPa of lengths 0.745 and 0.753 Å, respectively, expand slowly with pressure, reaching 0.753 and 0.758 Å at 300 GPa. Figure 1 shows that the molecules in the weakly bonded layers of *Pc* (and similarly for *Pbcn* and $C2$) form distorted hexagons. The structure evolves into the higher symmetry *Ibam* space group above about 350 GPa, in which the weakly bonded layers adopt the graphene structure. The shortest bond in *Pc* at 150 GPa of length 0.729 Å slowly contracts with increasing pressure, reaching 0.722 Å at 300 GPa. The bond lengths in the weakly bonded layers of *Pc*, however, change more rapidly with pressure. At 150 GPa the

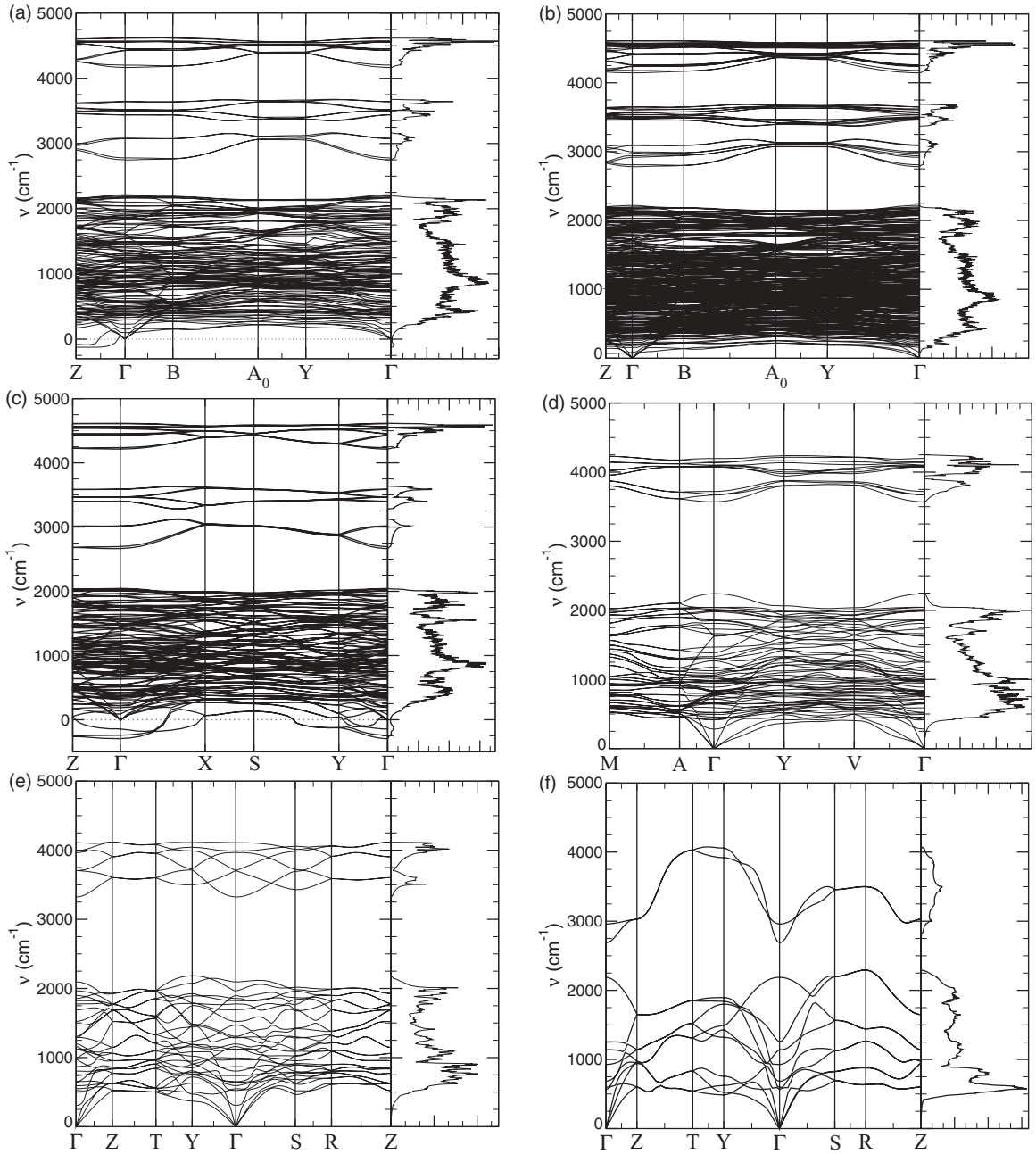

FIG. 3. (Color online) Phonon dispersion relations of (a) *Pc*, (b) *Pc*-96, (c) *Pbcn*, (d) $C2/c$, (e) *Cmca*-12, and (f) *Cmca*-4 at 250 GPa. The right-hand panels show the vibrational densities of states. The modes shown with negative frequencies indicate dynamical instabilities. The modes below 2500 cm^{-1} are lattice modes and those at higher frequencies are vibronic modes. The densities of states of the *Pc*, *Pc*-96, and *Pbcn* mixed phases are very similar and each has three distinct bands of vibrons. *Pc* has some unstable modes near Z while the unstable modes of *Pbcn* cover a substantial fraction of the zone. The *Pc*-96, $C2/c$, *Cmca*-12, and *Cmca*-4 structures are dynamically stable.

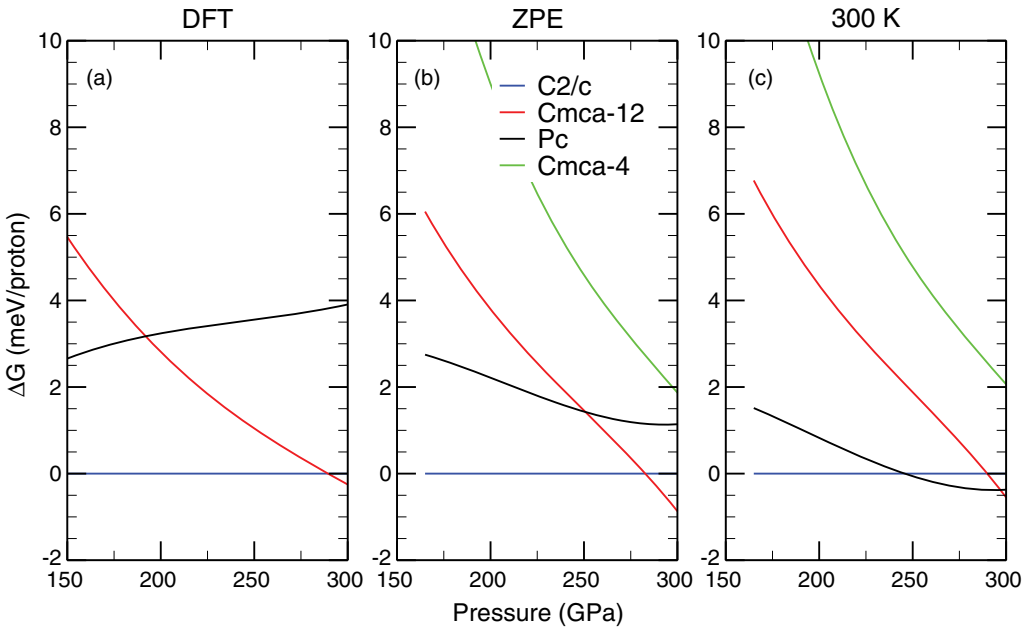

FIG. 4. (Color online) Enthalpies/free energies of the $Cmca$-12, Pc, and $Cmca$-4 structures relative to $C2/c$ for (a) the static lattice structures, (b) with proton ZP motion, and (c) with full vibrational motion at 300 K. The static-lattice enthalpy of $Cmca$-4 is too high for it to appear in (a).

weakly bonded layers have first and second nearest-neighbor distances of 0.763 and 1.175 Å, respectively, but upon further compression the shorter bonds expand and the longer ones contract, and at 300 GPa their bond lengths are 0.808 and 0.962 Å, respectively. These bond lengths become more nearly equal as the layer approaches the graphene structure.

C. Phonon calculations

We performed quasiharmonic vibrational calculations for the $C2/c$, $Cmca$-12, $Cmca$-4, $Pbcn$, and Pc phases; see Fig. 3. The $C2/c$, $Cmca$-12, and $Cmca$-4 phases are dynamically stable at 250 GPa, while the $Pbcn$ and Pc phases have some unstable modes. The unstable modes of $Pbcn$ cover a significant portion of reciprocal space, while Pc is lower in enthalpy than $Pbcn$ and has unstable modes over only a small region of reciprocal space. To investigate this further we doubled the unit cell of Pc to 96 atoms and re-relaxed, obtaining a Pc-96 structure[35] of the same symmetry that is slightly lower in enthalpy than Pc and has stable phonon modes (Fig. 3). The large size and low symmetry of the Pc-96 structure make it difficult to calculate accurate vibrational spectra, and therefore we used the Pc phase as our model for phase IV.

D. Enthalpy-pressure relations and phase diagram

We calculated the proton ZP energy of the $C2/c$, $Cmca$-12, $Cmca$-4, and Pc structures at several volumes and constructed the enthalpy at zero temperature both with and without ZP motion, and the Gibbs free energy at 300 K, as shown in Fig. 4. At the static lattice level, Pc is less stable than $C2/c$ over the pressure range covered by Fig. 4(a) and it becomes less competitive compared with $C2/c$ and $Cmca$-12 as pressure is increased. The $Cmca$-4 phase is more than 10 meV per proton higher in enthalpy than $C2/c$ at these pressures, and it is therefore not visible in Fig. 4(a). Including the vibrational ZP motion [Fig. 4(b)] changes the picture significantly as the Pc and $Cmca$-4 structures become more energetically competitive because they have lower vibrational frequencies than the strongly molecular $C2/c$ and $Cmca$-12 phases. Adding vibrational effects at a temperature of 300 K [Fig. 4(c)] results in the Pc phase becoming the most stable in the range 245–300 GPa. The corresponding phase diagram (Fig. 5) shows a region of stability for Pc that is compatible with the experimental data for phase IV. Below 260 K, we also find a transition from the $C2/c$ to $Cmca$-12 phases at about 285 GPa, which suggests the stability of another phase of molecular hydrogen at pressures beyond phase III.

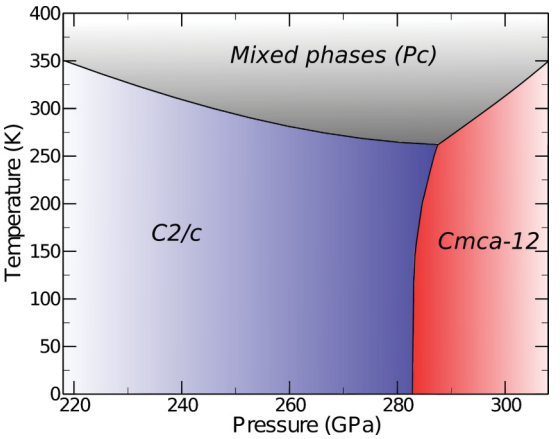

FIG. 5. (Color online) Computed phase diagram of hydrogen at high pressures.

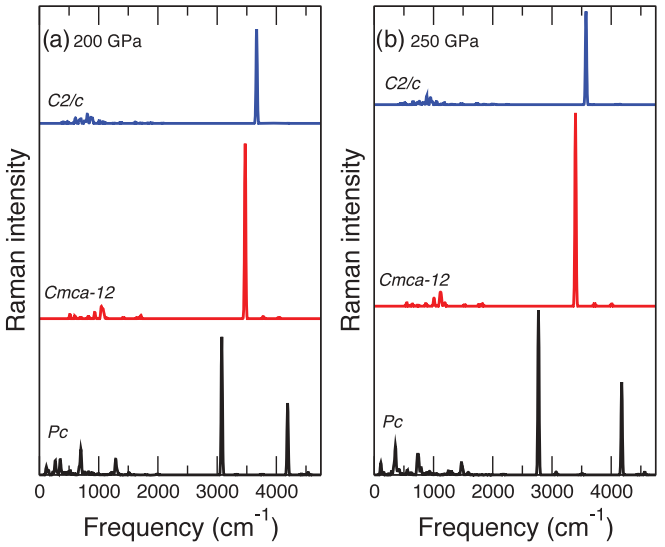

FIG. 6. (Color online) Raman spectra of $C2/c$, $Cmca$-12, and Pc at (a) 200 GPa and (b) 250 GPa.

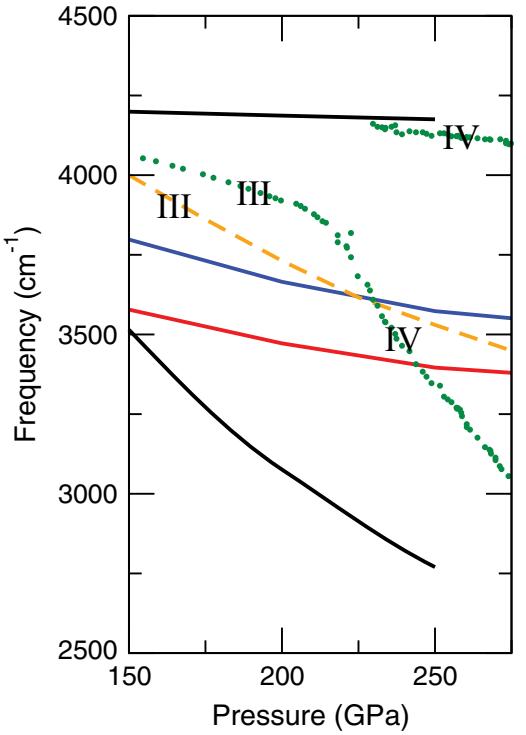

FIG. 7. (Color online) Pressure dependence of the Raman vibron frequencies of $C2/c$ (blue solid line), $Cmca$-12 (red solid line), and Pc (black solid line). The experimental data for phase III at 100 K (dashed orange line) are from Ref. 16 and the room temperature data for phases III and IV are from Ref. 15 (dashed green line).

E. Raman spectra

To investigate the possible relationship between phase IV and the most favorable structures obtained in our searches, we have calculated the frequencies and intensities of the Raman modes of $C2/c$, $Cmca$-12, $Cmca$-4, and Pc.[36,37] As can be seen in Figs. 6 and 7 and Table I, the $C2/c$ and $Cmca$-12 phases each have a single intense Raman vibron mode whose frequency slowly declines with pressure. The pressure dependence of the Raman vibronic frequency of $C2/c$ matches that observed for phase III reasonably well. The $Cmca$-4 structure[22] is not consistent with phase IV as it has a single intense Raman vibron mode at frequencies of about 3000 cm^{-1} which slowly declines with pressure and, as mentioned above, $Cmca$-4 is significantly less stable than other phases at 250 GPa. Pc has two strong vibronic Raman modes, one at just under 4200 cm^{-1} whose frequency is very weakly pressure dependent, and a second and more intense vibronic mode at lower frequencies which softens rapidly with increasing pressure; see Figs. 6 and 7 and Table I. Inspection of the vibrational eigenmodes shows that the higher frequency mode arises from the strongly bonded molecular layers while the lower frequency mode arises from the weakly bonded layers. Eremets and Troyan[14] did not discuss the less-intense higher-frequency Raman vibron mode of phase IV, but it is visible in Fig. 2(a) of their paper and in Fig. S3 of their supplementary information, and in the Raman data of Figs. 2 and 3 of Ref. 15. The higher frequency vibron of the Pc structure is a good match for the Raman mode of phase IV observed at about 4130 cm^{-1} in the range ∼220–250 GPa [see Fig. 2(a) of Ref. 14]. The higher experimental Raman vibron frequency and that calculated for Pc are almost independent of pressure in this range; see Fig. 6 and Table I.

TABLE I. Frequencies in cm^{-1} of the main IR and Raman peaks of $C2/c$, $Cmca$-12, and Pc as a function of pressure.

	IR					Raman						
$C2/c$												
200 GPa	1830	4150				3660						
250 GPa	1980	4080				3570						
300 GPa	2120	4030										
$Cmca$-12												
200 GPa	1380	1730	1940	3790	4030	1040	3470					
250 GPa	1470	1850	2090	3710	3970	1120	3400					
300 GPa	1550	1960	2230	3670	3940							
Pc												
200 GPa	1150	1850	3760	4520		120	270	350	700	1290	3060	4190
250 GPa	1200	1990	3520	4560		110	360	360	730	1470	2770	4170
300 GPa	1250	2110	3340	4600								

The experimental room temperature Raman data for hydrogen in Fig. 3 of Ref. 15 shows phase IV forming from phase III as the pressure is increased, see Fig. 7, which gives rise to the "knee" in the lower frequency vibron branch at around 220 GPa. The downward slope of the room temperature experimental data above 220 GPa[14,15] is in reasonable agreement with the calculated slope of the Raman data for the lower vibron mode of Pc, although the calculated modes are about 500 cm^{-1} lower in frequency; see Figs. 6 and 7 and Table I. The neglect of the effects of proton motion on the vibrational modes in our calculations might have a significant effect on the frequencies, as might the approximate density functional. The Pc structure does, however, yield qualitative agreement with the two Raman vibrons observed at room temperature in phase IV,[14,15] whereas the $C2/c$, $Cmca$-12, and $Cmca$-4 structures provide very poor descriptions.

The lattice Raman modes of $C2/c$, $Cmca$-12, and Pc extend to frequencies just above 2000 cm^{-1} at 250 GPa. Pc shows substantially higher lattice-mode Raman intensity than $C2/c$ or $Cmca$-12. $C2/c$ does not have any very strong lattice Raman modes, but $Cmca$-12 has a fairly intense mode at around 1100 cm^{-1}. The strongest peak in the lattice Raman modes of Pc is at 360 cm^{-1} at 250 GPa, with other peaks at 110, 730, and 1470 cm^{-1}. Phase IV shows three strong lattice-mode peaks at 250 GPa,[15] although peaks below about 150 cm^{-1} might be obscured by the filter. The strongest peak observed at 300 cm^{-1} is in reasonable agreement with our peak at 360 cm^{-1}, and the other two experimentally observed modes at 630 and 1065 cm^{-1} are in rough agreement with our calculated values of 730 and 1470 cm^{-1}. We find qualitative agreement between our calculated lattice Raman modes for Pc and those observed in phase IV,[15] whereas the $C2/c$, $Cmca$-12, and $Cmca$-4 structures provide very poor descriptions.

F. Infrared spectra

We have also calculated IR spectra for $C2/c$, $Cmca$-12, and Pc; see Fig. 8 and Table I. The vibronic modes of $C2/c$ and $Cmca$-12 soften with increasing pressure. $C2/c$ has a single intense IR vibron whose frequency drops with pressure from 4150 cm^{-1} at 200 GPa to 4030 cm^{-1} at 300 GPa. $Cmca$-12 has two intense IR vibrons at somewhat lower frequencies than the single intense vibronic mode of $C2/c$. The frequencies of the two intense IR vibrons of $Cmca$-12 are about 3790 and 4030 cm^{-1} at 200 GPa, and these frequencies fall to 3670 and 3940 cm^{-1}, respectively, at 300 GPa. Pc has two intense IR vibrons at 3760 and 4520 cm^{-1} at 200 GPa, but the intensity of the lower frequency mode falls rapidly with pressure, and at 300 GPa Pc has only a single intense IR vibron peak at 4600 cm^{-1}. The higher frequency IR vibron of Pc stiffens with pressure. The strength of the $Cmca$-12 IR vibron modes increases in comparison to those of $C2/c$ and Pc as pressure increases. The IR vibron of $C2/c$ is considerably more intense than those of Pc, and therefore we expect a drop in IR vibron intensity at the transition from phase III to IV.

As shown in Fig. 8 and Table I, the IR lattice modes of $C2/c$, $Cmca$-12, and Pc stiffen with increasing pressure. $C2/c$ has a single intense lattice mode whose frequency of 1830 cm^{-1} at 200 GPa increases to 2120 cm^{-1} at 300 GPa. This mode is in reasonable correspondence with observations for phase III of hydrogen. $Cmca$-12 has three intense lattice modes at 1380, 1730, and 1940 cm^{-1} at 200 GPa, which stiffen to 1550, 1960, and 2230 cm^{-1} at 300 GPa. Pc shows two intense lattice modes at 1150 and 1850 cm^{-1} which stiffen to 1250 and 2110 cm^{-1} at 300 GPa.

IR data for hydrogen up to 360 GPa and 250 K has recently been published.[38] According to our phase diagram (Fig. 5) none of the data sets in the lower part of Fig. 3 of Ref. 38 are within the region of stability of Pc, but the lower pressure data are within the region of $C2/c$ and the higher pressures data at (330 GPa, 100 K) and (360 GPa, 17 K) are within the region of $Cmca$-12. The drop in the observed IR vibron frequency visible in Fig. 3 of Ref. 38 of about 240 cm^{-1} between the data at (292 GPa, 200 K) and (330 GPa, 100 K) is consistent with a phase transition from $C2/c$ to $Cmca$-12, if the broadening of the peaks at 330 GPa and 360 GPa is taken to arise from the

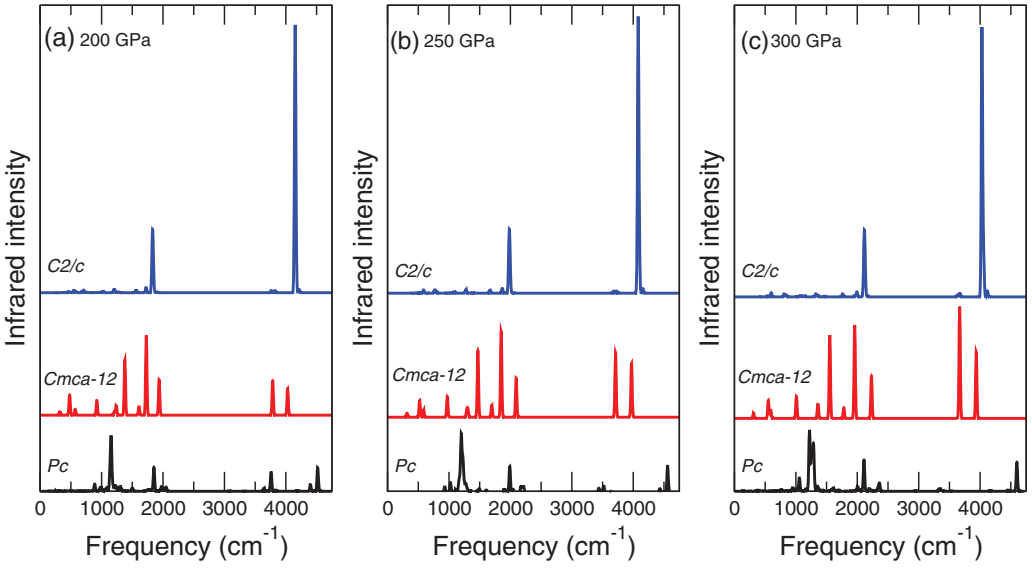

FIG. 8. (Color online) Infrared spectra of $C2/c$, $Cmca$-12, and Pc at (a) 200, (b) 250, and (c) 300 GPa.

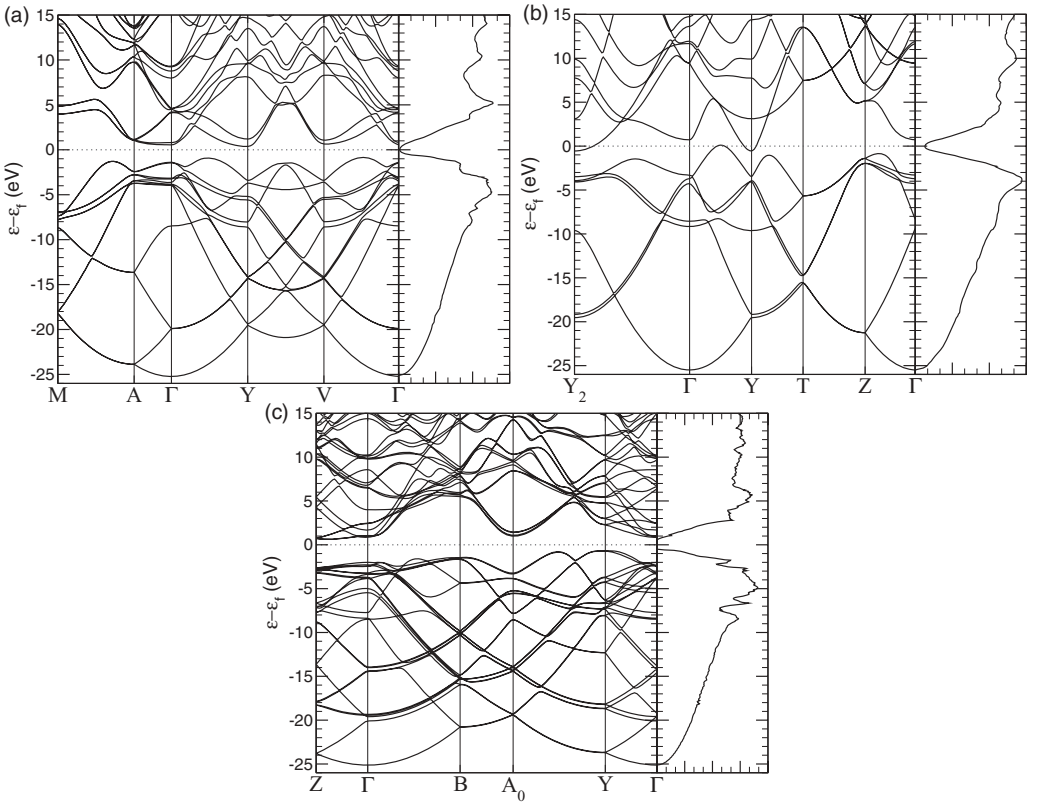

FIG. 9. (Color online) Electronic band structures of $C2/c$ (a), $Cmca$-12 (b), and Pc (c) at 250 GPa. The states below the blue horizontal line are occupied and those above are unoccupied. Note that the DFT calculations predict that $Cmca$-12 is slightly metallic at this pressure.

unresolved pair of vibronic peaks of $Cmca$-12, whose mean frequency is about 230 cm^{-1} lower than the vibron frequency of $C2/c$ at 300 GPa.

G. Band structures

The DFT band structures of $C2/c$, $Cmca$-12, and Pc at 250 GPa are shown in Fig. 9, and the pressure dependence of the band gaps is shown in Fig. 10. $Cmca$-12 has the smallest gap and Pc has the largest. The thermal (minimum) band gaps decrease with pressure and go to zero at 210 GPa ($Cmca$-12), 260 GPa ($C2/c$), and 320 GPa (Pc), while the optical band gaps (minimum direct gaps) are substantially larger. Standard DFT approaches, however, normally underestimate band gaps, and exact-exchange DFT calculations indicate that the true gaps may be roughly 1 eV larger.[39] Increasing the band gaps by 1 eV gives metallization pressures of about 250 GPa ($Cmca$-12), 310 GPa ($C2/c$), and 370 GPa (Pc). We have neglected the effect of nuclear vibrational motion on the band gaps, which is expected to be significant. The inclusion of vibrational motion is likely to reduce the band gap because it amounts to averaging the gap over the structures accessed during the motion, which are less stable than the static lattice structure and therefore tend to have smaller band gaps. This effect is expected to be significant in hydrogen because of the large vibrational amplitudes, and it may be particularly important in the weakly bonded layers of the Pc phase. The underestimation of the band gaps arising from the PBE functional may tend to be canceled by our neglect of the effects of coupling between the electronic and vibrational degrees of freedom. We cannot therefore obtain a reliable estimate of the gap at this level of theory but, if we suppose that the DFT calculations underestimate the band gap by 1 eV, we find that the coupling of the electronic and vibrational motion would have to reduce the gap by about 1 eV to reproduce the room temperature gap of phase IV of 1.8 eV at 315 GPa reported by Howie *et al.*[15] Theoretical work describing the anharmonic proton vibrations at finite temperatures and their effect on the

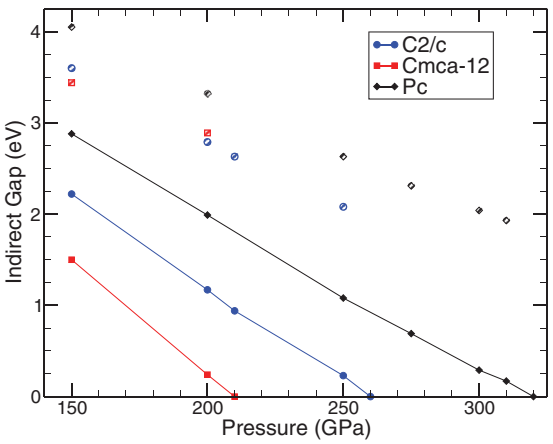

FIG. 10. (Color online) Band gaps of $C2/c$, $Cmca$-12, and Pc as a function of pressure. The solid symbols show the thermal (minimum) band gaps while the striped symbols represent the minimum optical (direct in k space) gaps.

structure and band gap will be required to investigate this in more detail.

IV. SUMMARY AND CONCLUSIONS

In summary, our results support the observation by Eremets and Troyan[14] and Howie *et al.*[15] of a structural phase IV of hydrogen at room temperature and pressures above 200 GPa. The $C2/c$, $Cmca$-12, and $Cmca$-4 candidate structures cannot account for the observed properties of phase IV. DFT calculations predict the Pc structure to be stable at room temperature over the pressure range 250–295 GPa, in reasonable agreement with the experimental observations of phase IV. Mixed structures are stabilized by the presence of low-frequency vibrational modes arising from the weakly bonded graphene-like layers. Mixed structures explain the observation of both the high-frequency Raman vibron of phase IV that is almost independent of pressure and arises from the short bonds in the strongly bonded layers, and the lower frequency vibron whose frequency falls rapidly with pressure, which arises from the weakly bonded layers. We find the $C2/c$ structure, which was previously identified as a candidate for phase III,[17] to be stable at low temperatures. The larger lattice-mode Raman intensity of Pc compared with that of $C2/c$ is also consistent with experiment, and we find qualitative agreement between the calculated lattice Raman modes of Pc and those observed for phase IV.[14,15] We conclude that mixed phases are reasonable structural models of phase IV of hydrogen.

ACKNOWLEDGMENTS

We acknowledge financial support from the Engineering and Physical Sciences Research Council (EPSRC) of the United Kingdom, and the use of the UCL Legion High Performance Computing Facility and associated support services. We thank Eugene Gregoryanz for helpful discussions.

*c.pickard@ucl.ac.uk

[1] J. Dewar, Ann. Chim. Phys. **18**, 145 (1899).
[2] E. Wigner and H. B. Huntington, J. Chem. Phys. **3**, 764 (1935).
[3] H.-K. Mao and R. J. Hemley, Rev. Mod. Phys. **66**, 671 (1994).
[4] I. I. Mazin, R. J. Hemley, A. F. Goncharov, M. Hanfland, and H.-K. Mao, Phys. Rev. Lett. **78**, 1066 (1997).
[5] N. W. Ashcroft, Phys. Rev. Lett. **21**, 1748 (1968).
[6] E. Babaev, A. Sudbo, and N. W. Ashcroft, Nature (London) **431**, 666 (2004).
[7] *The Extrasolar Planets Encyclopaedia*, [http://exoplanet.eu/].
[8] S. T. Weir, A. C. Mitchell, and W. J. Nellis, Phys. Rev. Lett. **76**, 1860 (1996).
[9] P. Loubeyre, R. LeToullec, D. Hausermann, M. Hanfland, R. J. Hemley, H.-K. Mao, and L. W. Finger, Nature (London) **383**, 702 (1996).
[10] Y. Akahama, M. Nishimura, H. Kawamura, N. Hirao, Y. Ohishi, and K. Takemura, Phys. Rev. B **82**, 060101 (2010).
[11] A. F. Goncharov, E. Gregoryanz, R. J. Hemley, and H.-K. Mao, Proc. Natl. Acad. Sci. USA **98**, 14234 (2001).
[12] P. Loubeyre, F. Occelli, and R. LeToullec, Nature (London) **416**, 613 (2002).
[13] M. Hanfland, R. J. Hemley, and H.-K. Mao, Phys. Rev. Lett. **70**, 3760 (1993).
[14] M. I. Eremets and I. A. Troyan, Nat. Mater. **10**, 927 (2011).
[15] R. T. Howie, C. L. Guillaume, T. Scheler, A. F. Goncharov, and E. Gregoryanz, Phys. Rev. Lett. **108**, 125501 (2012).
[16] Y. Akahama, H. Kawamura, N. Hirao, Y. Ohishi, and K. Takemura, J. Phys.: Conf. Ser. **215**, 012056 (2010).
[17] C. J. Pickard and R. J. Needs, Nat. Phys. **3**, 473 (2007).
[18] C. J. Pickard and R. J. Needs, Phys. Status Solidi B **246**, 536 (2009).
[19] C. J. Pickard and R. J. Needs, Phys. Rev. Lett. **97**, 045504 (2006).
[20] C. J. Pickard and R. J. Needs, J. Phys.: Condens. Matter **23**, 053201 (2011).
[21] R. J. Hemley, I. I. Mazin, A. F. Goncharov, and H.-K. Mao, Europhys. Lett. **37**, 403 (1997).
[22] K. A. Johnson and N. W. Ashcroft, Nature (London) **403**, 632 (2000).
[23] L. Pauling, J. Am. Chem. Soc. **51**, 1010 (1929).
[24] J. M. McMahon and D. M. Ceperley, Phys. Rev. Lett. **106**, 165302 (2011).
[25] C. J. Pickard and R. J. Needs, J. Chem. Phys. **127**, 244503 (2007).
[26] C. J. Pickard and R. J. Needs, Phys. Rev. Lett. **102**, 125702 (2009).
[27] C. J. Pickard and R. J. Needs, Nat. Mater. **7**, 775 (2008).
[28] A. D. Fortes, E. Suard, M.-H. Lemee-Cailleau, C. J. Pickard, and R. J. Needs, J. Am. Chem. Soc. **131**, 13508 (2009).
[29] S. J. Clark, M. D. Segall, C. J. Pickard, P. J. Hasnip, M. I. J. Probert, K. Refson, and M. C. Payne, Z. Kristallogr. **220**, 567 (2005).
[30] J. P. Perdew, K. Burke, and M. Ernzerhof, Phys. Rev. Lett. **77**, 3865 (1996).
[31] D. Vanderbilt, Phys. Rev. B **41**, 7892 (1990).
[32] H. J. Monkhorst and J. D. Pack, Phys. Rev. B **13**, 5188 (1976).
[33] P. Giannozzi, S. Baroni, N. Bonini, M. Calandra, R. Car, C. Cavazzoni, D. Ceresoli, G. L. Chiarotti, M. Cococcioni, I. Dabo, A. Dal Corso, S. Fabris, G. Fratesi, S. de Gironcoli, R. Gebauer, U. Gerstmann, C. Gougoussis, A. Kokalj, M. Lazzeri, L. Martin-Samos, N. Marzari, F. Mauri, R. Mazzarello, S. Paolini, A. Pasquarello, L. Paulatto, C. Sbraccia, S. Scandolo, G. Sclauzero, A. P. Seitsonen, A. Smogunov, P. Umari, and R. M. Wentzcovitch, J. Phys.: Condens. Matter **21**, 395502 (2009).
[34] J. S. Tse, D. D. Klug, Y. Yao, Y. Le Page, and J. R. Rodgers, Solid State Commun. **145**, 5 (2008).
[35] See Supplemental Material at http://link.aps.org/supplemental/10.1103/PhysRevB.85.214114 for crystallographic information.
[36] K. Refson, P. R. Tulip, and S. J. Clark, Phys. Rev. B **73**, 155114 (2006).
[37] D. Porezag and M. R. Pederson, Phys. Rev. B **54**, 7830 (1996).
[38] C.-S. Zha, Z. Liu, and R. J. Hemley, Phys. Rev. Lett. **108**, 146402 (2012).
[39] M. Städele and R. M. Martin, Phys. Rev. Lett. **84**, 6070 (2000).